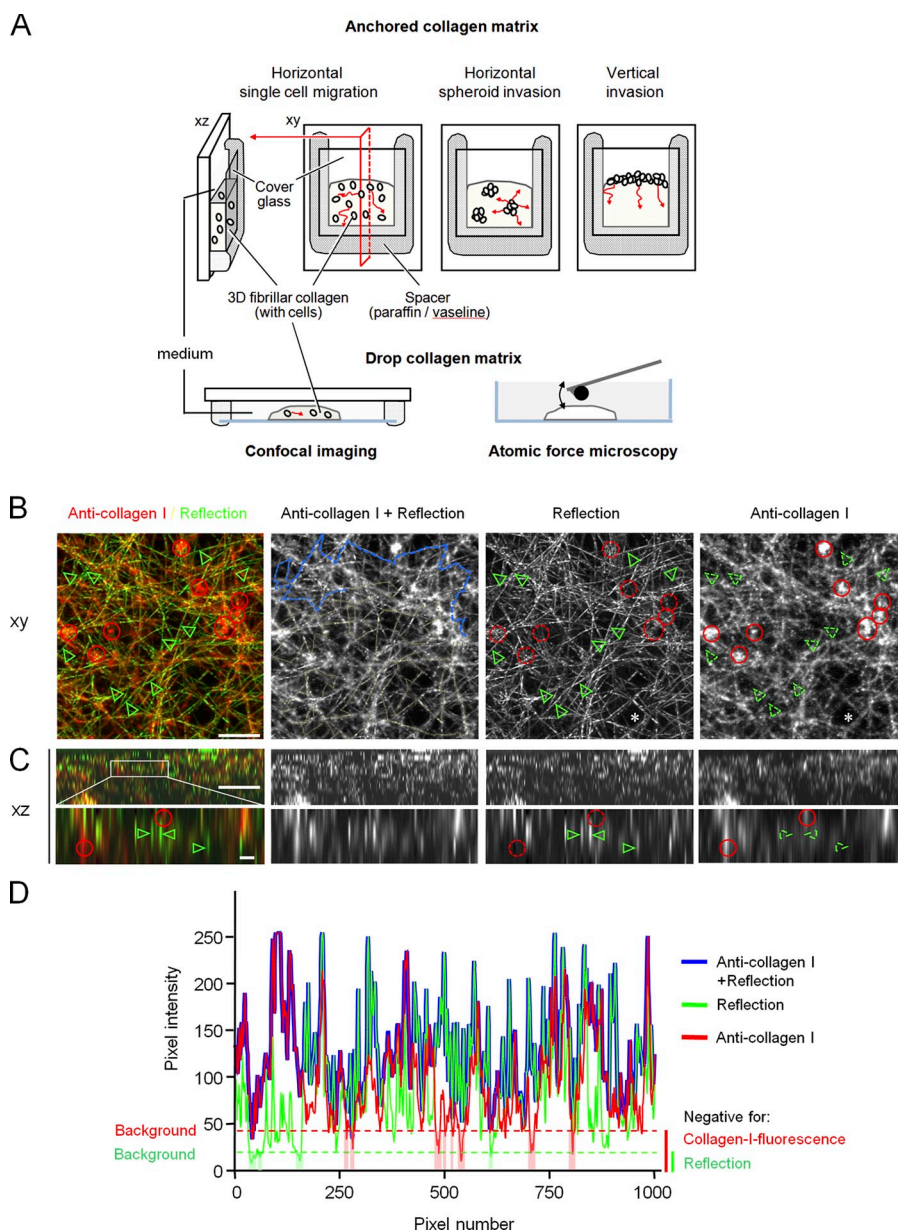


Wolf et al., <http://www.jcb.org/cgi/content/full/jcb.201210152/DC1>

merged fibrils consists of 1,000 pixels (see D) and illustrates the region of interest for image segmentation (totalling 7,177 pixels). (D) Pixel intensities of merged image as reference (blue), reflection (green), and fluorescence (red) channel. Signal-negative regions below background (intensity threshold: 20 pixel for reflection, green dotted line; 45 pixel for fluorescence, red dotted line) are displayed as shaded lines. Of 7,177 pixels analyzed, 97.2% were positive for reflection signal, and 90% for fluorescence signal. One representative experiment out of $n = 2$. Bars, 10 μm (except xz zooms, 1 μm).

Figure S1. 3D collagen models for cell migration analysis, optical imaging, and measurement of stiffness.

(A) (Top row) Cell-collagen mixtures were polymerized in vertical chamber position to ensure that cells slowly sinking downward during collagen assembly remained embedded within the 3D collagen scaffold and did not reach the collagen-glass interface (Friedl and Bröcker, 2004). The dual-glass interface further provided sufficient adsorption and anchorage of the collagen matrix to the chamber, preventing cell-mediated matrix contraction or spontaneous collapse of upper matrix layers in the vertical invasion assay. Cell migration was measured in three different assays: (1) migration of single cells embedded during collagen polymerization; (2) invasion from 3D multicellular spheroids embedded during collagen polymerization; or (3) vertical invasion from the top of a preformed 3D collagen lattice. Red arrows, cell migration tracks. (Bottom row) Drop gels embedded in closed chambers were used for confocal imaging of both fixed and live cell-collagen cultures (left), whereas drop gels in an open Petri dish were used for atomic force microscopy using a bead-functionalized cantilever (right). (B–D) Validation of confocal reflection microscopy for detecting collagen fibrils. (B) Merged and single-channel images of anti-collagen type-I immunofluorescence staining and reflection signal from hydrated 3D collagen fibril structures for comparison of loss of signal. 3D bovine collagen (1.7 mg/ml) was fixed with paraformaldehyde, stained with polyclonal rabbit anti-collagen type-I antibody, and scanned by confocal microscopy. xy images represent maximum intensity projections of three consecutive z-scans with each 2- μm distance. (C) Overview xz images and zoom of central regions. (B and C) To estimate the proportion of false-negative pixels using confocal reflection microscopy, anti-collagen staining and reflection signals were both cross-referenced for signal-negative regions. Red circles show fluorescence-positive (smooth line) but reflection-negative (dotted line) dots, consistent with rare fibrils oriented in vertical direction (Jawerth et al., 2010). Green arrowheads, reflection-positive fibrils (smooth line) with fluorescence signal below background (dotted line). Background was determined from fibril-free areas (asterisks). Blue line along

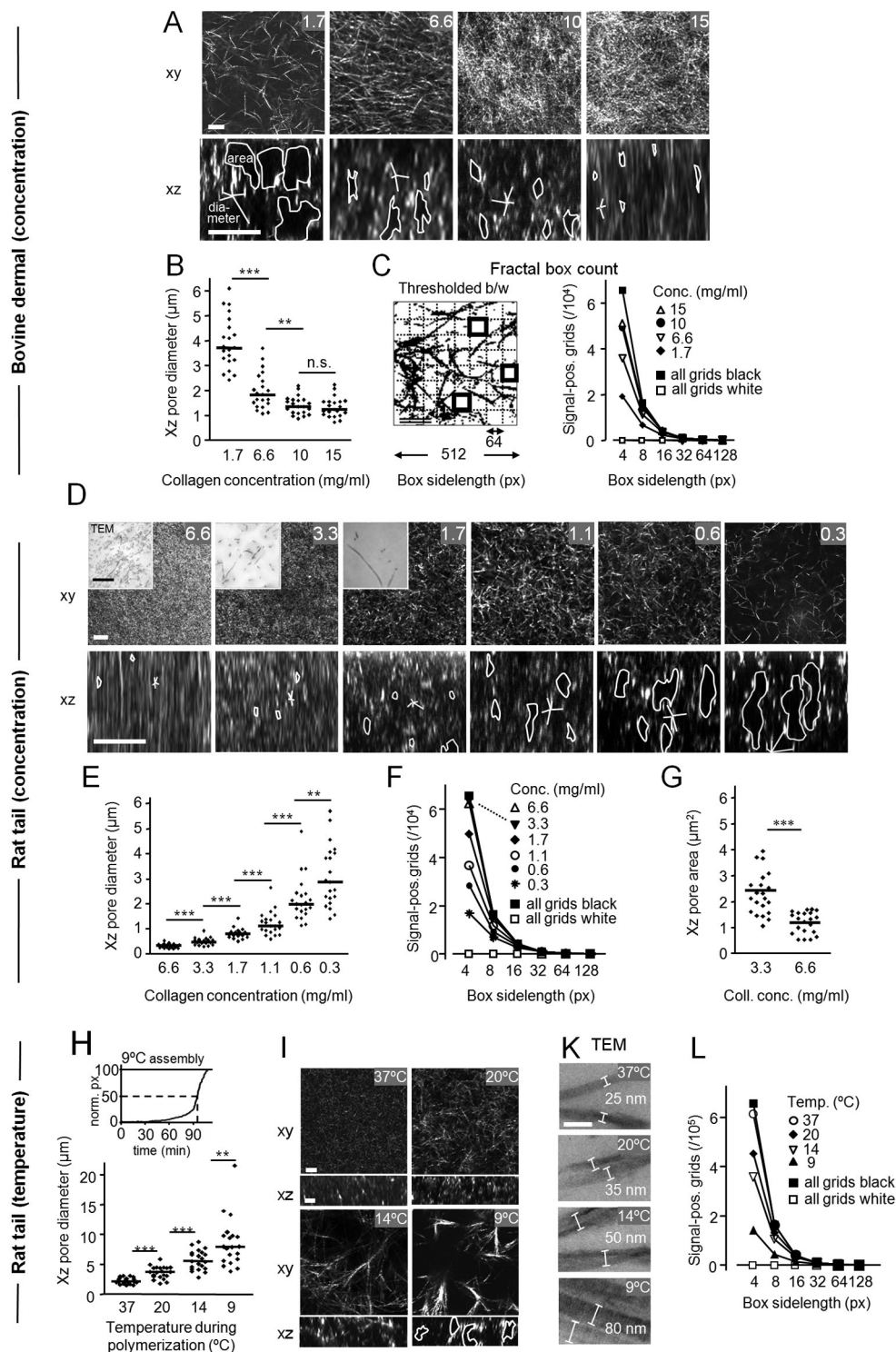


Figure S2. **Quantification of fibril organization and density of 3D collagen matrices reconstituted from bovine dermal and rat tail collagen.** (A, D, and I) Single xy and xz reflection scans from native hydrated collagen lattices used for image analysis. In xz scans, marked areas indicate examples of measured pore areas, and straight lines show examples of pore diameters. (B, E, and H [bottom]) Pore diameters obtained from xz sections (medians representing 21 data points per condition; $n = 2$). (C, F, and L) Overall porosity, quantified by fractal analysis from single xy sections. Fractal box count was performed by overlaying a thresholded image with grids decreasing in side length. Only those grid-encircled boxes were counted that contain reflection-positive signal, as a reciprocal measure for porosity (fractal box count plugin, Fiji software). (G) Pore cross sections for high-density rat tail collagen, calculated from xz images in D. (C, F, G, and L) One representative analysis out of $n = 2-3$. (D [insets] and K) Transmission electron microscopy images of collagen fibrils and fibers after polymerization at different concentration and temperature. (H, top) Assembly speed of rat tail collagen (1.7 mg/ml) at 9°C and half-maximum polymerization (dashed lines; after 96 min). ***, $P < 0.001$; **, $P < 0.01$; n.s., nonsignificant. Bars, 10 μm (all images) except 1 μm (D, insets) and 0.1 μm (K).

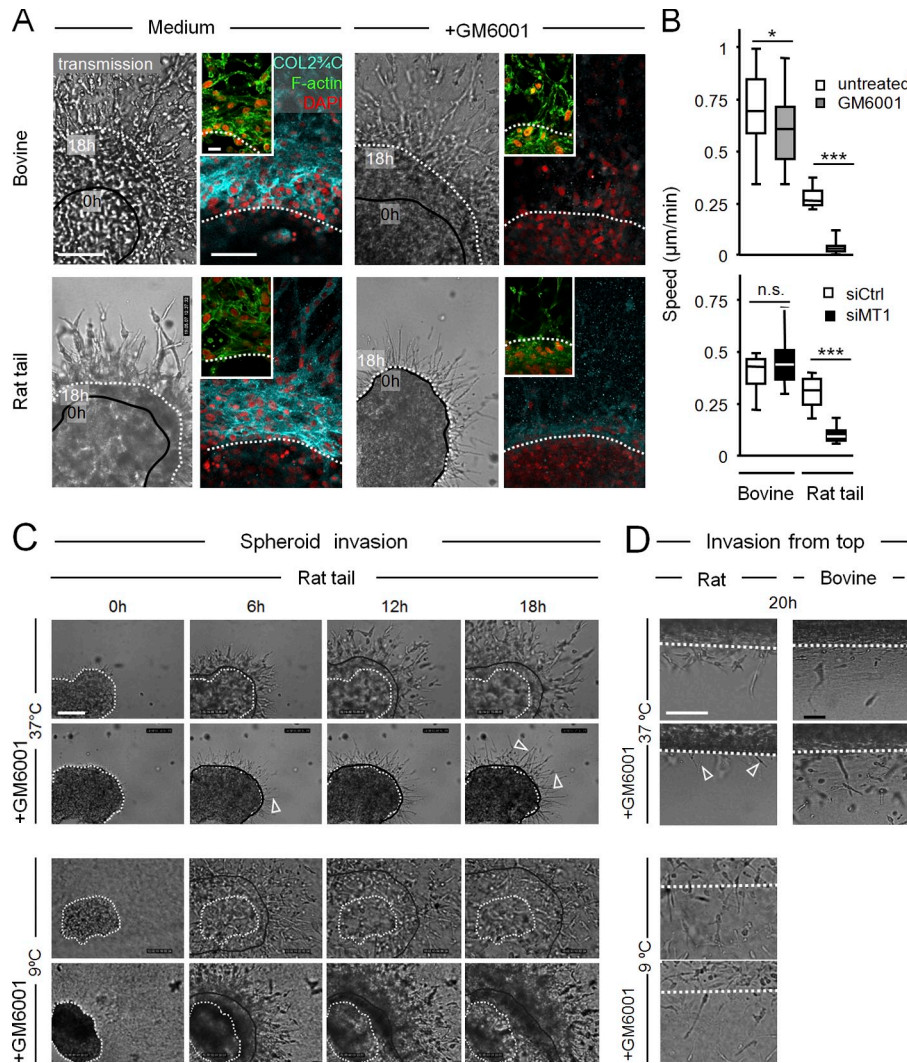


Figure S3. **Rate-limiting conditions of cell migration in 3D spheroid and vertical invasion assays.** (A) HT1080/MT1 spheroid invasion into bovine dermal or rat tail collagen (1.7 mg/ml) after 24 h in the absence or presence of MMP inhibitor GM6001. Black lines (transmission images) indicate tumor–collagen borders at 0 h (after collagen polymerization); white dashed lines show the noninvasive edge of the spheroids after 18 h migration, consistent with abrogation of proliferation in confining matrices in the absence of MMP activity (Hotary et al., 2003). Images are part of the time-lapse sequences shown in Video 3. For fluorescence imaging, samples were fixed with PFA, stained with DAPI, phalloidin, or COL23/4C_{short} Ab, three-dimensionally reconstructed by confocal microscopy, and displayed as maximum intensity projection. (B) Cell migration speed after emigration from spheroids into bovine dermal or rat tail collagen in the absence or presence of GM6001 (top), or after transient RNA knockdown of MT1-MMP (bottom). Box and whiskers represent the mean population speed per cell with median, 25th/75th, and 5th/95th percentiles (15–20 cells from one representative experiment). ***, $P < 0.0001$; *, $P < 0.05$; n.s., nonsignificant. (C) Spheroid invasion or (D) vertical invasion into rat tail collagen polymerized at 37°C or 9°C in the absence or presence of GM6001. As reference, vertical invasion into bovine dermal collagen was equally effective in the presence or absence of GM6001. Arrowheads indicate long cytoplasmic extensions as indicator for abrogated migration despite frustraneous leading edge dynamics. Bars, 100 μm (all images) except 20 μm (A, inset).

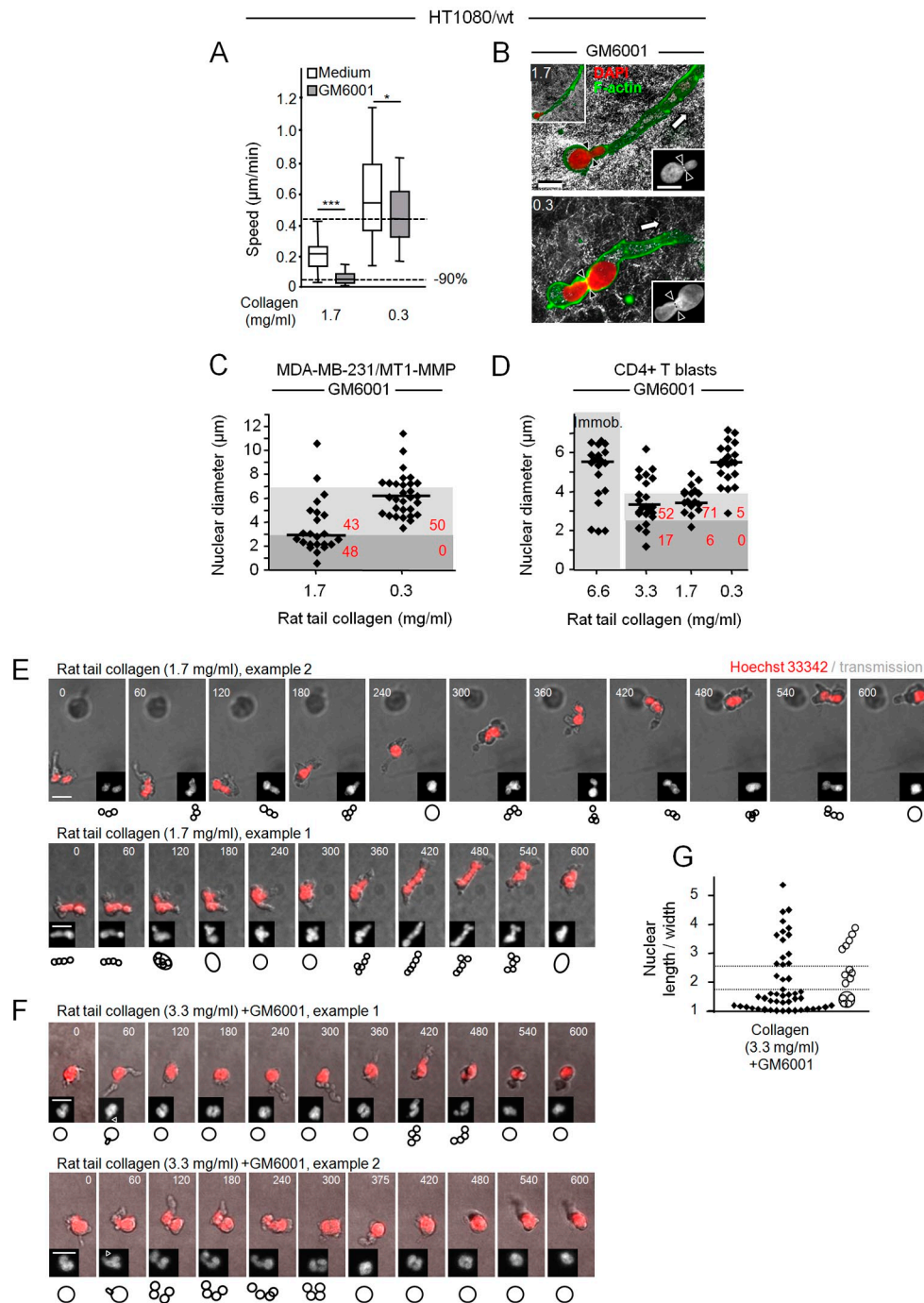
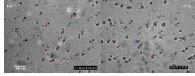
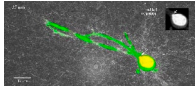


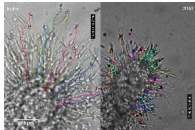
Figure S4. Speed and nuclear adaptation data from different cell types. Limits of MMP-independent migration and nuclear morphologies in HT1080/wt (A and B), MDA-MB-231/MT1 cells (C), CD4+ T-blasts (D), and PMNs (E–G). (A) Migration rates of HT1080/wt cells in the absence or presence of GM6001 in low- or high-density rat tail collagen. Top dashed line in A, 100% reference for MMP-independent migration; bottom dashed line, 90% inhibition of migration ($n = 4$). ***, $P < 0.0001$; *, $P < 0.05$. (B) Cellular including nuclear morphologies in HT1080/wt cells. Prolapse of the nucleus in direction of a prominent dendrite-like leading extension at conditions of migration arrest (1.7 mg/ml), whereas hour-glass shaped nuclear morphology is retained in moving cell (0.3 mg/ml). Arrowheads, region of nuclear deformation. Arrows, direction of cell protrusion or migration. (C and D) Deformation of nuclei in MDA-MB-231/MT1 cells (C) and CD4+ T-blasts (D) in low- or high-density rat tail collagen in the presence of GM6001 ($n = 2$, each 17–30 nuclei). Dark gray areas correspond to nuclei of immobilized cells. (E and F) Bright-field time-lapse sequences of PMNs stained with DNA marker Hoechst 33342 during migration in rat tail collagen of 1.7 (E) or 3.3 mg/ml (F) in the absence or presence of GM6001. Insets (grayscale) show the Hoechst channel (maximum intensity projections of three z-planes with 2- μm step size); symbols indicate the nuclear conformation and arrowheads indicate prolapse. (G) Length/width index of polymorphonuclear nuclei at high rat tail collagen density (3.3 mg/ml) that strongly decreased but did not abrogate migration in the presence of GM6001 (compare Fig. 4 F), showing the spectrum of nuclear shapes in slowly moving PMNs. 49 cells, $n = 2$. Bars, 10 μm .



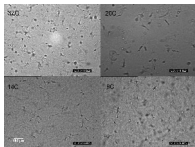
Video 1. **Spontaneous migration of HT1080/MT1 cells, and migration arrest after inhibition of MMP activity by GM6001 in 3D rat tail but not bovine dermal collagen.** Imaging by bright-field inverse microscopy (Leica) at 37°C. (A, first sequence) Overview movies of spontaneous HT1080/MT1 cell movement in bovine dermal (left) and rat tail collagen of 1.7 mg/ml (right); representative still images are shown in Fig. 2, A and C. Second clip: as first, plus 20 μ M GM6001. Cell tracks indicate the migratory capacity of each condition. Time (h:min:s) as indicated (24-min intervals over 18 h of observation).



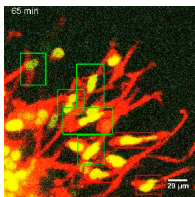
Video 2. **Confocal time sequence of migration arrest.** Single HT1080/dual-color cell expressing cytoplasmic DsRed2 (red) and nuclear histone-2B (H2B)-coupled EGFP (green) in rat tail collagen (1.7 mg/ml), in the presence of GM6001. White arrow highlights short-lived repeated prolapses of the nucleus in direction of the leading pseudopod. Imaging at 37°C by laser scanning confocal microscopy (510; Carl Zeiss) and maximum intensity projection of confocal z-stacks with 2.5-min time interval for 100 min.



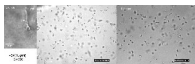
Video 3. **Emigration of HT1080/MT1 cells from multicellular spheroids into bovine (left) or rat (right) collagen (1.7 mg/ml) in the absence (A, first sequence) or presence (B, second sequence) of MMP inhibitor GM6001 with paths representing the position change of cell centers.** Representative still images are shown in Fig. S3 A. Bright-field inverse microscopy (Leica) at 37°C; time (h:min:s) as indicated (16-min intervals over 8.5 h of observation).



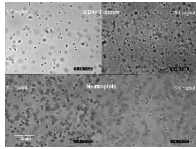
Video 4. **Rescue of MMP-independent migration of HT1080/MT1 cells in rat tail collagen (1.7 mg/ml) in the presence of GM6001 after reconstitution at different polymerization temperatures indicated in the movies.** Bright-field inverse microscopy (Leica) at 37°C. Time (h:min:s) as indicated (32-min intervals over 22 h of observation).



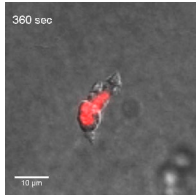
Video 5. **Nuclear deformation together with ongoing or abrogated migration of HT1080 cells transfected with histone H2B-GFP and cytoplasmic DsRed2 in the presence of protease inhibitors.** Deformation of the nucleus in spheroid culture of HT1080 dual-color cells expressing cytoplasmic DsRed2 (red) and nuclear histone-2B (H2B)-coupled EGFP (green) during migration (cells in green boxes) or immobilization (red boxes) in bovine collagen (6.6 mg/ml) in the presence of MMP and other protease inhibitors (see Materials and methods). Imaging at 37°C by confocal microscopy (SP2; Leica); maximum intensity projection of confocal z-stacks; 5-min frame rate, 85-min observation time.



Video 6. **Abrogation and physical rescue of nonproteolytic HT1080/MT1 cell migration after interference with cell-matrix adhesion and contractility in bovine dermal collagen lattices of increasing pore sizes.** Imaging at 37°C by bright-field inverse microscopy (Leica). Cells migrating in the presence of GM6001 were additionally treated with 4B4 mAb (1 μ g/ml; A, first video sequence) or Y-27632 (2 μ M; B, second sequence). (A and B) Left, collagen concentration 1.7 mg/ml (high magnification); middle, 1.7 mg/ml; right, 0.8 mg/ml. Time intervals as indicated.



Video 7. **Migration of CD4⁺ T-blasts and PMNs in rat tail collagen at low and high concentrations indicated in the movie in the presence of MMP-inhibitor GM6001.** Imaged at 37°C by bright-field inverse microscopy (Leica); time (h:min:s) as indicated (2-min frame interval; 2 h of observation).



Video 8. **Pearl chain configuration of segmented nucleus during neutrophil migration in rat tail collagen (1.7 mg/ml) in the presence of IL-8 (100 ng/ml).** Maximum intensity projection of red DNA label (Hoechst 33342 dye) with transmission image obtained by time-lapse confocal microscopy (LSM510; Carl Zeiss). Frame interval, 15 s; duration, 10 min.

References

- Friedl, P., and E.B. Bröcker. 2004. Reconstructing leukocyte migration in 3D extracellular matrix by time-lapse videomicroscopy and computer-assisted tracking. *Methods Mol. Biol.* 239:77–90.
- Hotary, K.B., E.D. Allen, P.C. Brooks, N.S. Datta, M.W. Long, and S.J. Weiss. 2003. Membrane type I matrix metalloproteinase usurps tumor growth control imposed by the three-dimensional extracellular matrix. *Cell*. 114:33–45. [http://dx.doi.org/10.1016/S0092-8674\(03\)00513-0](http://dx.doi.org/10.1016/S0092-8674(03)00513-0)
- Jawerth, L.M., S. Münster, D.A. Vader, B. Fabry, and D.A. Weitz. 2010. A blind spot in confocal reflection microscopy: the dependence of fiber brightness on fiber orientation in imaging biopolymer networks. *Biophys. J.* 98:L1–L3. <http://dx.doi.org/10.1016/j.bpj.2009.09.065>